JACS
JOURNAL OF THE AMERICAN CHEMICAL SOCIETY

Article

pubs.acs.org/JACS

Old Metal Oxide Clusters in New Applications: Spontaneous Reduction of Keggin and Dawson Polyoxometalate Layers by a Metallic Electrode for Improving Efficiency in Organic Optoelectronics

Maria Vasilopoulou,*[,†] Antonios M. Douvas,[†] Leonidas C. Palilis,[‡] Stella Kennou,[§] and Panagiotis Argitis[†]

[†]Institute of Nanoscience and Nanotechnology (INN), National Center for Scientific Research "Demokritos", 15310 Aghia Paraskevi Attikis, Athens, Greece

[‡]Department of Physics, University of Patras, 26500 Patras, Greece

[§]Department of Chemical Engineering, University of Patras, 26500 Patras, Greece

Supporting Information

ABSTRACT: The present study is aimed at investigating the solid state reduction of a representative series of Keggin and Dawson polyoxometalate (POM) films in contact with a metallic (aluminum) electrode and at introducing them as highly efficient cathode interlayers in organic optoelectronics. We show that, upon reduction, up to four electrons are transferred from the metallic electrode to the POM clusters of the Keggin series dependent on addenda substitution, whereas a six electron reduction was observed in the case of the Dawson type clusters. The high degree of their reduction by Al was found to be of vital importance in obtaining effective electron transport through the cathode interface. A large improvement in the operational characteristics of organic light emitting devices and organic photovoltaics based on a wide range of different organic semiconducting materials and incorporating reduced POM/Al cathode interfaces was achieved as a result of the large decrease of the electron injection/extraction barrier, the enhanced electron transport and the reduced recombination losses in our reduced POM modified devices.

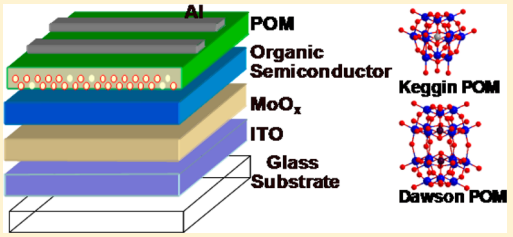

INTRODUCTION

In view of increasing environmental and economic pressure to use renewable sources for energy and lighting applications, optoelectronic devices based on organic semiconductors (OSCs) look like potentially attractive technological tools. This could explain the current rapid development of organic photovoltaics (OPVs) and organic light emitting diodes (OLEDs) as they offer the promise of low-cost flexible solar cells, displays, and light sources that have the potential to be manufactured on large-area plastic substrates.[1−8] One of the key elements for improving efficiencies in organic optoelectronics is finding suitable cathode electrode materials to replace the reactive low work function metals, such as calcium or magnesium, that are typically used to either inject electrons into or extract electrons from the lowest unoccupied molecular orbital (LUMO) of a given OSC.[9−11] Several approaches have been explored the most common of which is the use of an electron transport material between a higher work function but air stable cathode electrode (such as aluminum, Al) and a semiconducting layer in the device. Common examples of this approach have included n-type metal oxide films, such as ZnO and TiO_2,[12−15] chemisorbed self-assembled monolayers (SAMs) of dipolar molecules,[16−18] aggregates of porphyrin/phthalocyanine derivatives,[19,20] inorganic based modifiers, such as Cs_2CO_3,[21] conjugated polyelectrolytes,[22,23] and polar solvents,[24,25] which can substantially enhance electron injection/extraction rates when spin-coated onto the OSC surface. All these materials, which are chemically or physically adsorbed onto the OSC surface, are chosen in such a way as to exhibit solution processability, adequate electronic conductivity and create strong interface and/or molecular dipoles that induce a vacuum-level shift and modify the work function of the OSC underneath.[26]

It is therefore straightforward to conclude that our ability to manipulate the structure and functions of novel materials at wish carries the prospect of applications previously not considered in the realm of organic optoelectronics technology. Nevertheless, while evolutionary materials and methods seem the most fertile approach for novel devices such as organic optoelectronics, the capabilities of de novo design are expanding. And emerging applications of already existing materials may be a key tool for materials science in the century ahead. Polyoxometalates (POMs), for instance, are a well-known large group of clusters with frameworks built from transition metal oxo anions linked by shared oxide ions, first reported by Jöns Jacob Berzelius in 1826.[27,28] Their precise molecular structure was first unraveled by J. F. Keggin in

Received: February 20, 2015
Published: May 7, 2015

DOI: 10.1021/jacs.5b01889
J. Am. Chem. Soc. 2015, 137, 6844−6856

1933,[29] while, nowadays, it has been confirmed that virtually all $[XM_{12}O_{40}]^{m-}$ -type POMs (X = P, Si, Al, etc.; M = Mo,W, V, etc.) feature the so-called Keggin structure, where a central XO_4^{3-} tetrahedral group is surrounded by 12 fused MO_6 octahedrons sharing oxygens at their edges or vertices. Other relevant POM structures, such as the larger Dawson ($[X_2M_{18}O_{62}]^{n-}$) structure, have been extensively studied as well.[30−32] In recent years, thanks to combined experimental and theoretical efforts, a variety of POMs properties are fairly well understood.[33−35] One of the most intriguing properties of POM clusters is their high ability to accept a large number of electrons with minimal structural modifications, a property that enables them to play an important role as catalysts,[36,37] single-molecule magnets[38] and, recently, as cathode-active materials in rechargeable batteries.[39,40] This property also means that POMs have the potential for the design of molecular clusters capable of high reduction, which enables the delocalization of a large number of electrons allowing them to play an important role as excellent electron conductors in electronic devices. Previously, our group introduced the use of the Keggin phosphotungstic acid ($H_3PW_{12}O_{40}$) as a novel electron injection/extraction layer in OLED/OPV devices,[41,42] whereas Y. Yang et al. also demonstrated enhanced photovoltaic response when incorporating a polyoxometalate into a phthalocyanine-sensitized electron extracting electrode.[43] On the other hand, other POMs have been recently incorporated by other groups as hole extraction layers in organic solar cells.[44−46] The improvement of the devices efficiency was ascribed to the fine energy level matching and to suppressed charge recombination at the anode contact. Note that in those cases all POMs exhibited their metallic addenda atoms in their fully oxidized state. These conflicting results raise the question of which members of the plethora of POM clusters and under what conditions may find successful application as interelectrode materials in organic optoelectronics.

We report here on the preparation of efficient electron transport interlayers consisting of highly reduced POM clusters spin coated from a methanol solution between the organic active layer and Al electrode for application in organic optoelectronics. A high degree of reduction was enabled for POMs via spontaneous electron transfer from the Al electrode to their low lying lowest unoccupied molecular orbital (LUMO). We report remarkable enhancement of OLEDs and OPVs efficiency when using the reduced POM/Al cathodes, which was attributed to the formation of an Ohmic contact thus promoting electron injection/transport and the suppression of recombination losses. Our methodology was used in several state-of-the-art devices including OLEDs based on the green emitting poly[(9,9-dioctylfluorenyl-2,7-diyl)-*co*-(1,4-benzo-{2,1′,3}-thiadiazole)] (F8BT) and a wide range of OPV devices based on photoactive layers composed of mixtures of a polymer donor, such as poly(3-hexylthiophene) (P3HT), poly[(9-(1-octylnonyl)-9*H*-carbazole-2,7-diyl)-2,5-thiophenediyl-2,1,3-benzothiadiazole-4,7-diyl-2,5-thiophenediyl] (PCDTBT) or poly({4,8-bis[(2-ethylhexyl)oxy]benzo[1,2-b:4,5-b′]dithiophene-2,6-diyl}{3-fluoro-2-[(2-ethylhexyl)-carbonyl] thieno[3,4-b]thiophenediyl}) (PTB7), and a fullerene acceptor, such as [6,6]-phenyl C71 butyric acid methyl ester ($PC_{71}BM$).

EXPERIMENTAL SECTION

Preparation of POM Materials and POM Films. The Keggin POMs $H_4SiW_{12}O_{40}$ (hereinafter referred to as POM 1), $H_3PW_{12}O_{40}$ (POM 2) and $H_3PMo_{12}O_{40}$ (POM 4) were purchased from Sigma-Aldrich. The mixed addenda $H_5PV_2W_{10}O_{40}$ (POM 3) and Dawson POMs $(NH_4)_6P_2W_{18}O_{62}$ (POM 5) and $(NH_4)_6P_2Mo_{18}O_{62}$ (POM 6) were prepared according to the literature.[47] POM films were deposited via spin coating at 6000 rpm for 30 s from a methanol (MeOH, obtained from Sigma-Aldrich) solution. The concentration of Keggin POMs was optimized at 10 mg/mL (for efficient device operation), while that of the Dawson POMs was 5 mg/mL, resulting in the formation of relatively smooth films with a thickness of 2−3 nm.

Devices Preparation. All solution processed OLEDs and OPVs were fabricated on oxygen plasma-cleaned indium tin oxide (ITO) coated glass substrates. Substoichiometric molybdenum oxide (MoO_x) films about 20 nm thick were deposited via a recently reported solution processing method,[48] to serve as anode interfacial layers to improve hole injection. Next, in OLED devices, an ∼80 nm thick layer of the green-yellow emitting polyfluorene copolymer F8BT (obtained from American Dye Source Inc.) was spin-cast on MoO_x from an 8 mg/mL chloroform solution. Prior to spin coating, the polymer solution was filtered using a 0.20 μm PTFE filter. After spin coating, the emissive layer was annealed at 85 °C for 10 min in air. Next, a thin POM interlayer (∼2−3 nm) was deposited from a methanolic solution on the polymer film to serve as the electron conducting (injecting) layer in the OLED configuration. OPV devices were fabricated on oxygen plasma-cleaned ITO-coated glass substrates (2 × 2 cm^2), which served as the anode electrode. The MoO_x hole extraction layer with a thickness of approximately 20 nm was then deposited, followed by an approximately 100 nm photoactive layer. The active layer consisted of either P3HT:$PC_{71}BM$ blend (1:0.8 wt % ratio) or PCDTBT:$PC_{71}BM$ (1:4 wt % ratio) or PTB7:$PC_{71}BM$ (1:1.5 wt % ratio) and it was spin-cast on top of the MoO_x interlayer from a 20 mg mL^{-1} chlorobenzene solution (+3% 1,8-diiodoctane (DIO) for the PTB7-based blends). After spin coating, the active layer was annealed either at 130 °C (P3HT:$PC_{71}BM$) or at 70 °C (PCDTBT:$PC_{71}BM$ and PTB7:$PC_{71}BM$) for 10 min in air. Then, a ∼2−3 nm POM interlayer was inserted to serve as the electron extraction layer. The devices were completed with a 150 nm thick aluminum anode, deposited in a dedicated chamber. All chemicals were purchased from Sigma-Aldrich and used with no further purification.

Measurements and Instrumentation. The current density−voltage characteristics of the fabricated OLEDs and OPVs were measured with a Keithley 2400 source-measure unit. Luminance and electroluminescence (EL) spectra were recorded with an Ocean Optics USB 2000 fiber optic spectrophotometer, assuming a Lambertian emission profile (for luminance measurements). For the photocurrent measurements the OPV devices were illuminated with a xenon lamp and an AM1.5G filter to simulate solar light illumination conditions with an intensity of 100 mW/cm^2. To accurately define the active area of all devices we used aperture masks during the measurements with areas equal to those of the Al contacts (12.56 mm^2). The measurements were performed in air and at room temperature. Absorption measurements were taken using a PerkinElmer Lampda 40 UV/vis spectrophotometer. The thickness of the organic and the POM films was measured with an Ambios XP-2 profilometer and a M2000 Woolam ellipsometer, respectively. For the chemical analysis of the pristine POMs, samples were prepared by spin coating a ∼10 nm POM film onto a p-type Si substrate, whereas for the analysis of the reduced POMs films were deposited on p-type Si substrates covered with a thin (∼10 nm) Al layer. The analysis was performed with X-ray photoelectron spectroscopy (XPS) measurements with a hemisherical analyser Leybold EA 11. The spectra were obtained after excitation using Mg Kα (1,253.6 eV) radiation of a twin anode in a constant analyzer energy mode with pass energy of 100 eV. All binding energies were referred to the C 1s peak at 284.8 eV and to the O 1s peak at 530.2 eV of the surface adventitious carbon and oxygen, respectively. The stoichiometry of POMs was estimated using the XPS-measured W 4f, Mo 3d and V 2p core levels, respectively, and the corresponding O 1s photoemission peaks. To this extent, the areas under the photoemission peaks were integrated by fitting the O 1s and W 4f (or Mo 3d, V 2p) spectra with asymmetric Gaussian−Lorentzian curves. The raw data, after a Shirley background subtraction, were

DOI: 10.1021/jacs.5b01889
J. Am. Chem. Soc. 2015, 137, 6844−6856

fitted by a nonlinear least-squares routine using peaks with a mix of Gaussian and Lorentzian shapes. The error is estimated at ±10% in all the XPS-derived atomic percentages. For the determination of valence band and work function of POMs ultraviolet photoelectron spectroscopy (UPS) measurements were performed using the He I (21.22 eV) excitation line. A negative bias of 12.28 V was applied to the samples during UPS measurements in order to separate the sample and analyzer high binding energy (BE) cut-offs and estimate the absolute work function value from the secondary electron cutoff region of the UPS spectra. The analyzer resolution is determined from the width of the Au Fermi edge to be 0.16 eV. Regarding the UPS measurements, because the high intensity UV photons used may alter the surface of POM films, we adopted a certain protocol for the measurement of their work function: we first measured the core levels and work function of the sample using low intensity X-rays and then we measured the work function with UPS to verify that the samples have remained unaffected. IPCE measurements were carried out using an Autolab PGSTAT-30 potentiostat, with a 300 W Xe lamp in combination with an Oriel 1/8 monochromator for dispersing the light in an area of 0.5 cm^2. A Thorlabs silicon photodiode was used for the calibration of the IPCE spectra. The capacitance−voltage measurements were recorded on devices exhibiting the same architecture as described above (OPVs) at a frequency of 100 kHz and an AC bias of 25 mV by using a Keithley 4200−SCS DC characterization system. The measurements were performed in air at room temperature. Transient photocurrent measurements were performed by photogenerating carriers in solar cells through illumination from the ITO side by a 7 ns pulse of Nd:YAG laser (Quanta-Ray PRO-170, Spectra Physics) at 532 nm excitation wavelength. The laser system was running at a repetition rate of 2.177 Hz, and a fluence of 3.75 mW cm^{-2}. In order to improve the signal-to-noise ratio, the transient photocurrent data were obtained by an average of up to 100 measurements. The cells were biased with an Agilent 33519B waveform generator operating in DC mode.

RESULTS AND DISCUSSION

Monitoring the Spontaneous Reduction of POM films by Aluminum. We performed our study by selecting four representative members of the Keggin series having either different heteroatoms (X) or addenda atoms M ($XM_{12}O_{40}^{m-}$ where X = P, Si, and M = Mo, W, or mixed V, W addenda) and the Dawson counterparts of two of our Keggin POMs ($X_2M_{18}O_{62}^{n-}$ where X = P and M = Mo, W). The typical structural types of the POM clusters used in this study are shown in Figure 1. The reason for our selection can be explained as follows: an important property of the polyoxometalate anions is that their identity is usually preserved by reduction processes, forming reduction products (upon absorbance of UV or near-visible light) by addition of various

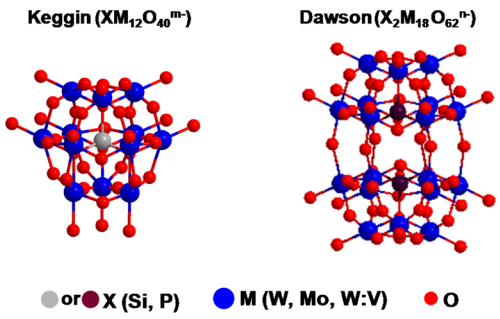

Figure 1. Molecular structures of Keggin and Dawson polyoxometalates (POMs) used in this study. The Keggin POMs are $H_4SiW_{12}O_{40}$ (POM 1), $H_3PW_{12}O_{40}$ (POM 2), $H_5PV_2W_{10}O_{40}$ (POM 3) and $H_3PMo_{12}O_{40}$ (POM 4), while the Dawson POMs are $(NH_4)_6P_2W_{18}O_{62}$ (POM 5) and $(NH_4)_6P_2Mo_{18}O_{62}$ (POM 6).

electrons which are delocalized over numerous centers of the polyoxoanion framework.[49−51] The reduction of each POM cluster depends on the nature and energy of its lowest unoccupied molecular orbitals (LUMOs).[52,53] The relative energy and composition of the LUMO correlate quite well with the electron affinity of each isolated M^{n+} ion that is in the order $Nb^{5+} < W^{6+} < V^{5+} < Mo^{6+}$. When the M^{m+} is substituted by a more electronegative ion, the energy of the LUMO decreases and the cluster is more easily reduced with the additional electron going to a metallic orbital. On the other hand, the total charge of the anion depends also on the heteroatom substitution.[52] In the dodecatungstates, for instance, the substitution of Si with P means that they are, in general, more easily reduced. Finally, the transformation of a XM_{12} into a X_2M_{18} decreases the energy gap between the highest occupied molecular orbital (HOMO) and LUMO orbitals by lowering the LUMO, making the cluster more easily reducible by a standard reductant. In the present study, Al was used as a reducing agent for POM. The selection of Al was made because it represents the most common air-stable metal cathode material for organic optoelectronic applications. The degree of reduction of POMs in Al/POM interfaces and the number of additional electrons per cluster were derived following changes in UV−vis absorption spectra of ∼10 nm POM films spin coated on Al layers (thinner than 10 nm in order to be transparent) deposited on quartz substrates. In addition, the same POM films were directly spin coated on pristine quartz substrates. Results are shown in Figure 2. In the spectra of POMs with the Keggin structure and W addenda atoms (POM 1-POM 2) the longer wavelength absorption peak at around 270 nm (Figure 2a, d), is ascribed to oxygen-to-metal charge transfer (OMCT).[53,54] Two peaks are clearly shown in the case of the mixed addenda POM (POM 3) corresponding to CT to W and V, respectively (Figure 2c). The long wavelength peak is shifted at longer wavelength in the case of the POM with Mo addenda atoms (POM 4) if compared with the corresponding POMs with W addenda atoms (Figure 2d). On the other hand, separation of the OMCT band in two shoulders and spectrum extension to the visible is observed in the case of the POM with the Dawson structure and W addenda atoms (POM 5). Finally the spectrum of the POM with Dawson structure and Mo addenda atoms (POM 6) is very similar to the corresponding POM with Keggin structure (POM 4) (Figure 2e, f). Note that the absorption spectra of the above materials exhibit no peaks in the visible wavelength region, as expected for fully oxidized POMs.[54] However, the situation is completely different for POM interfaces with Al; a broad band appears in the visible region of all spectra which is attributed to intervalence-charge transfer (IVCT) indicating the formation of reduced POM species (heteropoly blues).[55−59] In particular, in the case of POM 1 on Al a broad IVCT band located at ∼628 nm appears (Figure 2a), which indicates the reduction of POM with approximately two electrons per cluster according to literature.[54,55] Similar IVCT bands appear in the spectra of all POMs on Al with the intensity and mainly the position of those bands indicating the different degree of POMs reduction; thus, the IVCT band at ∼657 nm indicates the two electron reduction of POM 2 (Figure 2b), whereas the bands at 629 and 640 nm witness the four electron reduction of POMs 3 and 4 on Al (Figures 2c and d).[55−57] Similar behavior was also observed with POMs 5 and 6 on Al; the position of the IVCT bands at 570 and 591 nm (Figures 2e, f), respectively, indicates that in both cases approximately six electrons have been

DOI: 10.1021/jacs.5b01889
J. Am. Chem. Soc. 2015, 137, 6844−6856

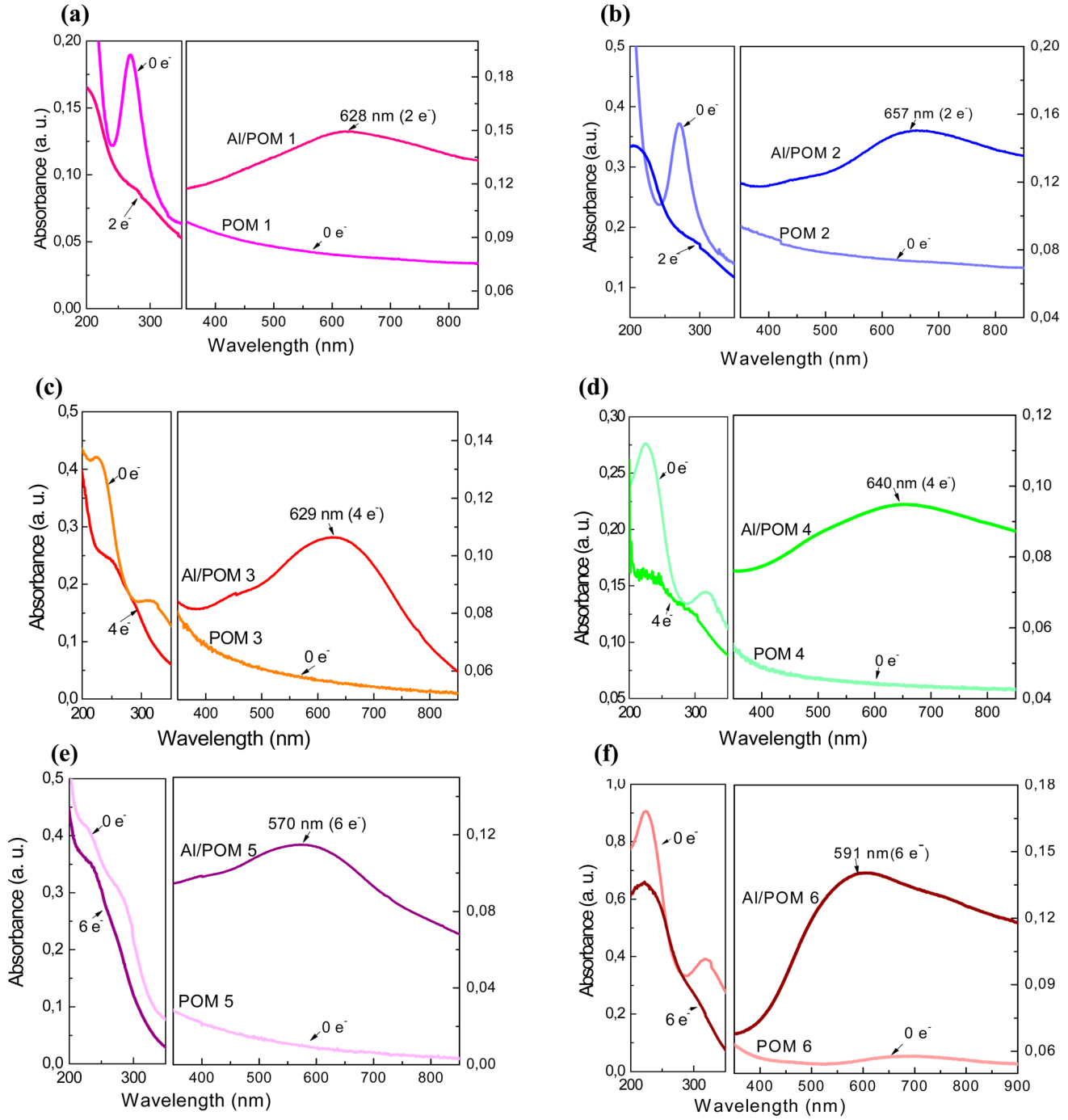

Figure 2. Absorption spectra of (a) POM 1, (b) POM 2, (c) POM 3, (d) POM 4, (e) POM 5 and (f) POM 6 on their oxidized (POM) and reduced (Al/POM) forms.

transferred into the POM clusters from the Al reductant.[58,59] Note that in all cases the intensity of the near-UV absorption OMCT bands decreases upon reduction, as expected.[60,61]

The reduction of POM layers deposited on Al substrates was also followed by monitoring the oxidation states of M centers with core-level X-ray photoelectron spectroscopy (XPS). Figure 3 shows the XPS spectra of ~10 nm thick POM films deposited on Al. The W 4f photosignals of the XPS spectra of the tungsten-based POMs 1, 2, 3, and 5 on Al are presented in Figure 3a, b, c and e, respectively. The deconvolution of the W 4f photoemission peaks was performed using two distinct doublets with the major contribution coming from the doublet with peaks of nearly equal width with the binding energy (BE) of W $4f_{7/2}$ centered at 36.0 ± 0.1 eV and that of W $4f_{5/2}$ at a BE of 38.2 ± 0.1 eV (with a peak ratio of 4:3). The position and the shape of these peaks are representative of W atoms with an oxidation state +6.[62] In addition, a second doublet at lower BEs (BE of W $4f_{7/2}$ = 34.8 eV, and of W $4f_{5/2}$ = 37.1 eV with a peak ratio 4:3) is also evident, which was attributed to the presence of W^{5+} ions, indicating that these films are reduced (exhibiting tungsten atoms with a valence of +5). The contribution of this second doublet in the overall photoemission peaks is quite similar in the cases of POMs 1, 2, and 3 indicating nearly the same degree of reduction whereas increases substantially for

DOI: 10.1021/jacs.5b01889
J. Am. Chem. Soc. 2015, 137, 6844−6856

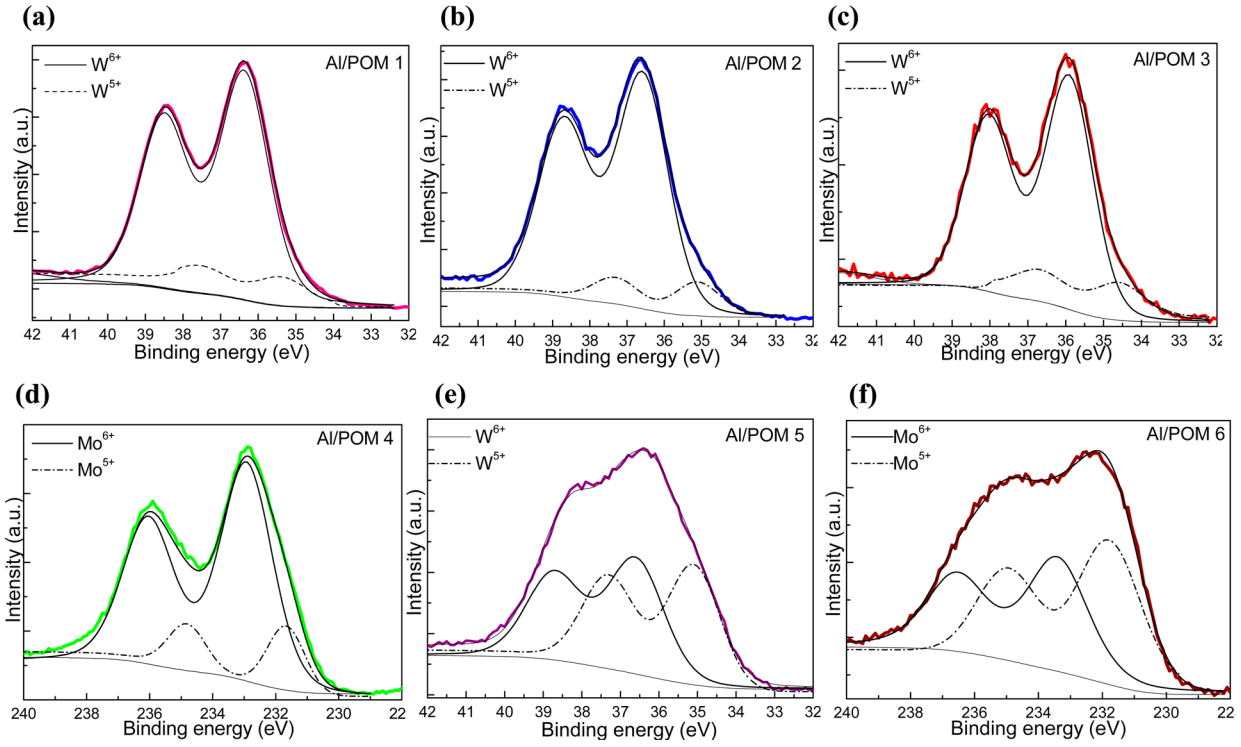

Figure 3. (a), (b), (c), (e) XPS W 4f core levels taken on 10 nm thick films consisting of POM 1, POM 2, POM 3, POM 5, respectively, deposited on Al substrates. (d) and (f) XPS Mo 3d core levels of Al/POM 4 and Al/POM 6 films, respectively.

POM 5. This is in good agreement with the UV-vis absorption spectroscopy results for POMs 1, 2, and 5 and again shows that the deposition on Al causes the reduction of the POM cluster. However, because a higher degree of reduction was concluded from the analysis of UV−vis absorption spectra of POM 3 on Al we also analyzed the V $2p_{3/2}$ photoemission peak of its XPS spectrum (Figure S1, Supporting Information) to gain more insight into the reduction process. It was found that this peak can be fitted satisfactorily with two nearly equivalent components with 517.2 and 516 eV BEs, respectively, characteristics of the fully oxidized (V^{5+}) and the reduced (V^{4+}) vanadium atoms.[63] This strongly suggests that, not only part of W atoms but also half of the V atoms are in a reduced state in the case of Al/POM 3 interface. This is in agreement with the four electron reduction of POM 3 on Al concluded from the UV−vis absorption study. Next, the reduction of molybdenum containing POMs was monitored using their XPS Mo 3d photoemission peaks shown in Figures 3 d and f for POMs 4 and 6 on Al, respectively. The data collected can be fitted with two pairs of 3d components. The first component has Mo $3d_{5/2}$ and Mo $3d_{3/2}$ with BEs of 232.5 and 235.5 eV, respectively, which is attributed to fully oxidized (Mo^{6+}) Mo atoms.[64,65] The second component has Mo $3d_{5/2}$ and Mo $3d_{3/2}$ with BEs of 231.6 and 234.9 eV, respectively, characteristic of the reduced (Mo^{5+}) molybdenum.[65] The contribution of the second component is very high in the case of Al/POM 6 interface, which means that the molecular transformation of the POM cluster from Keggin to Dawson type forces the reduction to proceed even further, as expected according to the above discussion. Note that the analysis of the XPS spectra of pristine POM samples (deposited on p-type Si substrates, Figure S2) revealed that the metal centers in those clusters exist in their highest oxidation state, therefore indicating that the clusters are fully oxidized. This shows that only deposition of POMs on Al substrates causes the spontaneous reduction of the cluster shell by a number of electrons dependent on the type of the cluster.

In order to gain more insight into the reduction of POMs by Al we next performed ultraviolet photoemission spectroscopy (UPS) measurements. The UPS spectra of 10 nm thick films consisting of POMs 1 to 6 deposited on Al substrates are shown in Figure 4a−f, respectively. The work function (W_F) of each sample surface can be directly obtained by measuring the secondary electron cutoff of the photoemission spectra, which gives a W_F value around 5.7−5.8 eV. By adding the BE of the onset of the band of occupied orbitals (also called as the *oxo band*) the ionization energy (I_E) of each POM was estimated (having values between 7.9 and 8.3 eV depending on the type of the cluster) which gives the position of the highest occupied molecular orbital (HOMO) with respect to the vacuum level. On the basis of the UPS results and the energy gap values estimated by Tauc plot analysis of absorption measurements taken on the same films (Figure S3) a molecular orbitals scheme for each POM studied here is presented in Figure S4, whereas in Figure 4g the energy levels of all POMs are summarized and compared with the Fermi level of Al (which is equal to 4.3 eV). For simplicity reasons vacuum level alignment is considered. It is concluded that in all cases the LUMO level of POMs lies below the Fermi level of Al. This means that in all cases the transfer of up to two electrons from Al to the LUMO of each POM cluster is energetically favored as shown in Figure 4g. In addition, as Miras et al. and Muller et al. have predicted, the energy of the LUMO+1 is at most ∼0.60−0.70 eV above their LUMO in the Keggin POMs (POMs 1−4) whereas in the W Dawson POM (POM 5) its LUMO+2 is placed ∼0.80 eV above its LUMO and in the Mo Dawson POM (POM 6) its LUMO+2 is placed at ∼0.60 eV above its LUMO.[66,67] Taking these theoretical calculations into account we assume that in POMs 3 and 4 except of their LUMO also their LUMO+1

DOI: 10.1021/jacs.5b01889
J. Am. Chem. Soc. 2015, 137, 6844−6856

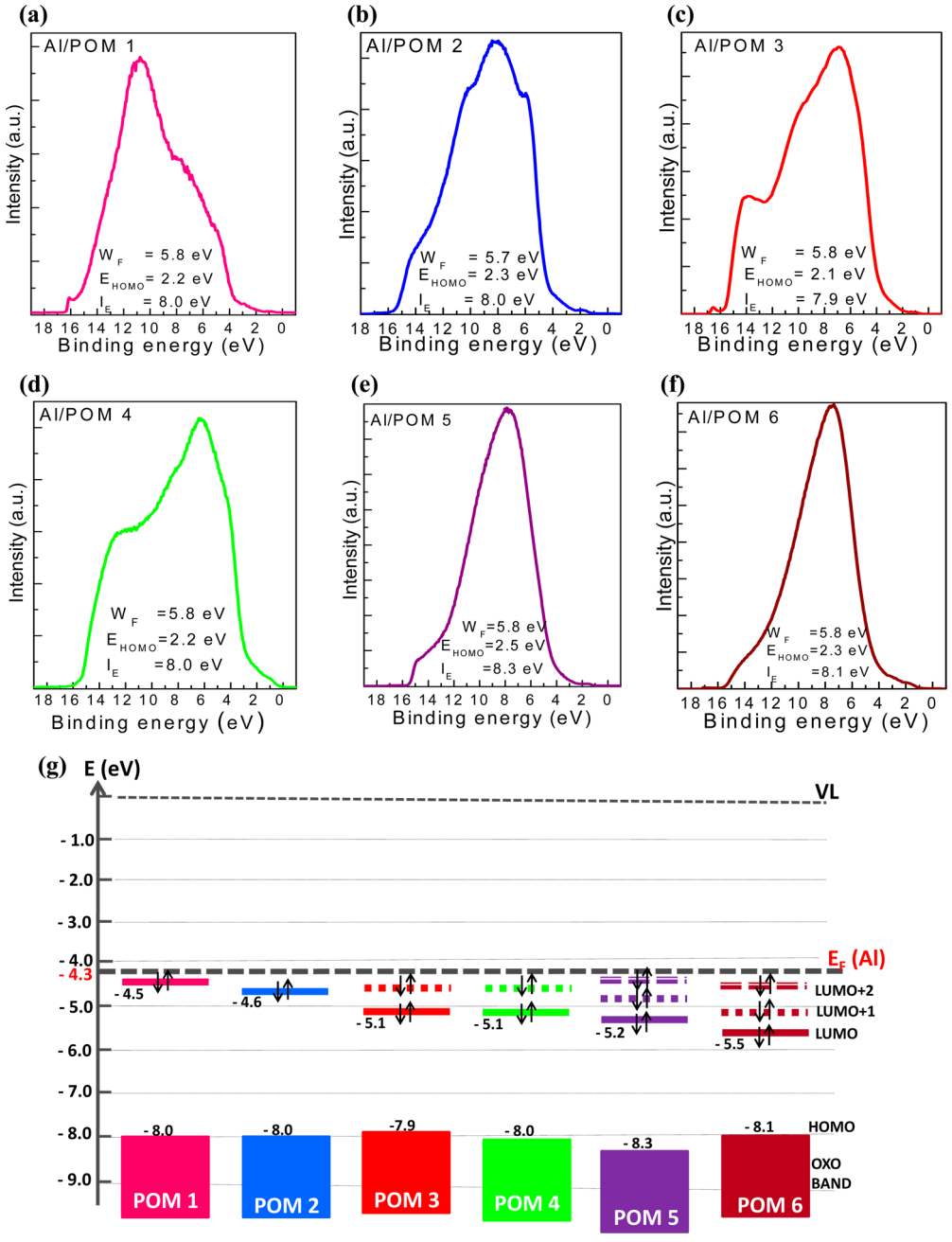

Figure 4. UPS photoemission spectra of 10 nm films consisting of (a) POM 1, (b) POM 2, (c) POM 3, (d) POM 4, (e) POM 5 and (f) POM 6 deposited on Al substrates. (g) Molecular orbital diagrams of POMs used in this study as derived from UPS and absorption measurements.

levels (estimated at ~4.4−4.5 eV) are placed below the Fermi level of Al whereas in POMs 5 and 6 even their LUMO+2 levels (estimated ~4.4 eV in POM 5 and ~4.9 eV in POM 6) are expected to lie below E_{FAl}. These assumptions could explain the spontaneous transfer of four electrons from Al to POMs 3 and 4 and of six electrons to POMs 5 and 6, concluded from the UV study shown above. More importantly, according to the orbital diagram presented in Figure 4g, the spontaneous reduction of some of the POMs studied here could be performed not only by using Al but also with higher work function materials such as indium tin oxide (ITO, W_F = 4.7 eV) and gold (Au, W_F = 5.3 eV), both of which are commonly employed as electrodes in the field of organic optoelectronics. Consequently, our approach of solid state electrochemical reduction of POMs by metal electrodes might be universal and may find applications in several types of devices where the high electron interfacial transfer in cathode interfaces is deemed necessary, such as optoelectronics, photocatalytic devices, and lithium batteries.

POMs as Electron Injection Layers in OLEDs. Next, we employed a ~2−3 nm POM film on top of an organic semiconductor, such as F8BT, to serve as cathode interlayer in OLEDs using Al as the cathode electrode. Note that an extensive study on the film forming properties of POMs when deposited via spin-coating on top of the surface of F8BT was deemed necessary in order to find process conditions allowing good coverage of the underlayer by a relatively smooth POM film. It was found that the process conditions are very crucial and that smooth films without any pinholes could be obtained when POMs were spin-coated from a concentrated methanol

DOI: 10.1021/jacs.5b01889
J. Am. Chem. Soc. 2015, 137, 6844−6856

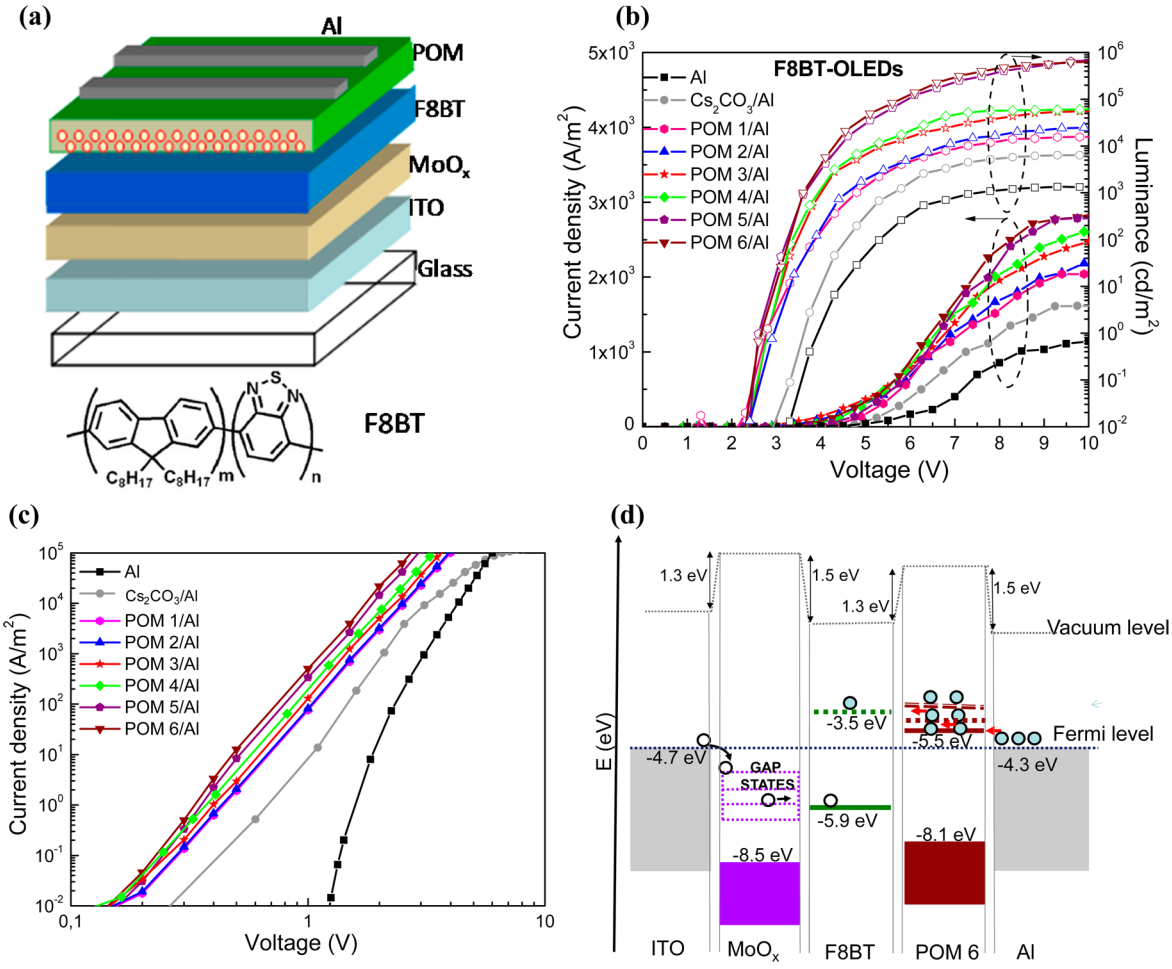

Figure 5. (a) Schematic architecture of the OLED devices with the structure ITO/MoO_x/F8BT/POM/Al. The chemical structure of the green emissive F8BT is also shown. (b) Current density–voltage (solid symbols, linear plot) and luminance–voltage (open symbols, log plot) characteristic curves of OLEDs using F8BT as the emissive component and various cathode interfaces. (c) *J*–*V* characteristics of the electron-only F8BT-based devices without and with an electron injection interlayer. (d) Energy level alignment in various interfaces of the F8BT-based OLED device as derived from UPS measurements. The free barrier electron injection at the reduced POM/Al cathode interface, is also illustrated. Solid and empty cycles are symbols for electrons and holes, respectively.

solution at high speed rotation (Figure S5 and discussion). The OLED device structure was ITO/MoO_x/organic semiconductor/POM/Al, where the ~20 nm MoO_x film was used as the anode interfacial layer to enhance hole injection, while the organic semiconductor was the green emitting F8BT copolymer.[68] The device architecture and the chemical structure of F8BT are presented in Figure 5a. In Figure 5b the current density–voltage–luminance (*J*–*V*–*L*) characteristics for F8BT-OLED devices using a POM electron injection layer (EIL), are shown. In addition, two reference devices, the one without any EIL and the other using the commercially available cesium carbonate (Cs_2CO_3) to facilitate electron injection, were fabricated and measured for comparison reasons. The detailed measurements taken from those devices are summarized in Table S1. It is observed that the reference device without any EIL exhibits a rather large turn-on voltage (voltage where light emission is equal to 10 cd/m^2) of about 3.5 V and an overall low emission (with a peak luminance of ~5000 cd/m^2) and max current density (of ~2000A/m^2). On the contrary, in the devices with the POM EILs nearly 2 orders of magnitude higher peak luminances and increased current densities are obtained, depending on the type of the POM cluster, accompanied by a large decrease in the device turn-on voltage. In particular, the device with the POM 6 as EIL reaches luminance values up to nearly 61500 cd/m^2 and current densities of 4400 A/m^2, while it also exhibits a low turn-on voltage of 2.5 V. The peak current efficiency of 14.0 cd/A represents one of the best values reported for thin (<100 nm) F8BT-based OLEDs.[26,69] It is of high importance to note that the performance of our OLED devices is directly related to the degree of reduction of POM-based EIL. Devices based on the moderately reduced POMs 1 and 2 perform much better compared with the reference device without an EIL and even exhibit higher efficiencies relative to the device bearing the commercially available cesium carbonate. The devices with the more reduced POMs 3 and 4, however, exhibit higher efficiencies, whereas our devices with the highly reduced POMs 5 and 6 are among the champion devices of their kind. As all OLED devices studied here exhibit the same anode interfaces and emissive layer we assume that the improved performance of OLEDs using POM/Al cathodes could be the result of enhanced electron injection/transport. The influence of POMs insertion on the electron injection efficiency of the devices was verified by fabricating electron only devices with the structure Al (150 nm)/F8BT (70 nm)/POM (2–3 nm)/Al (150 nm), whereas reference devices with a bare Al cathode or

DOI: 10.1021/jacs.5b01889
J. Am. Chem. Soc. 2015, 137, 6844–6856

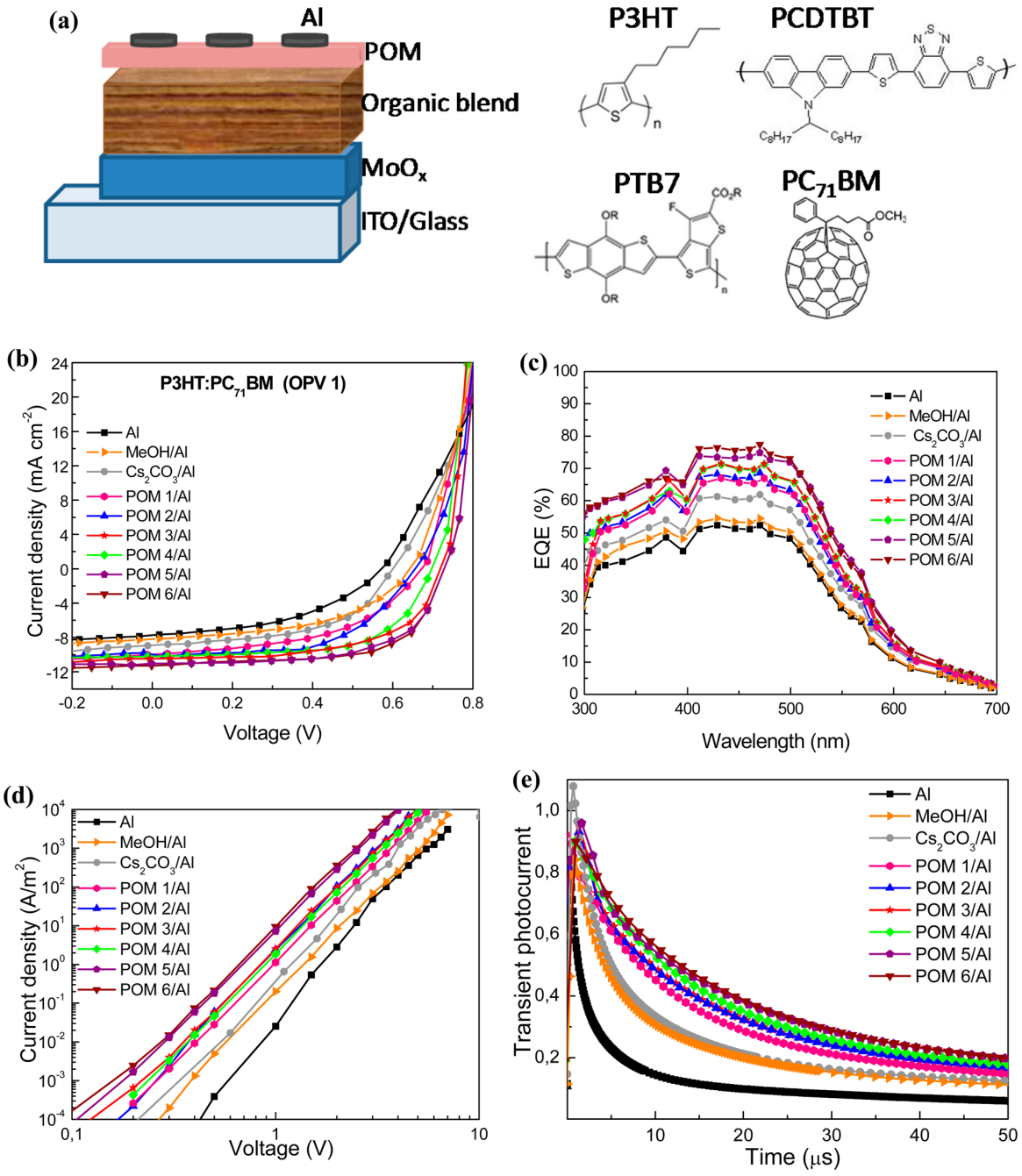

Figure 6. (a) Layer sequence of the OPVs based on different donor:acceptor blends with varied cathode interlayers. The molecular structures of the organic semiconductors used are also shown. (b) $J-V$ characteristics for P3HT:$PC_{71}BM$ based OPV 1 devices using various cathode interfaces. (c) The corresponding EQE curves. (d) $J-V$ curves in double-logarithmic scale obtained in electron-only P3HT:$PC_{71}BM$-based devices with various cathode interfaces, measured in the dark. (e) Transient photocurrent of P3HT:$PC_{71}BM$-based devices with various cathode interfaces near the maximum power point.

with a Cs_2CO_3 EIL, were also fabricated. From the comparison of the current density–voltage ($J-V$) characteristics of these devices (Figure 5c) became evident that the current in the reference device without any EIL is injection limited while in those with an EIL and, especially, with POMs is space charge limited verifying the formation of an Ohmic contact in the latter case. It is observed that the electron current of the F8BT/POM/Al devices is up to even 3 orders of magnitude higher than that of the F8BT/Al device while there is a correlation between the degree of POM reduction and the electron current density verifying the critical role of the reduction of POMs in the alteration of interfacial electron injection/transport. We have analyzed our electron-only devices using a space-charge-limited current (SCLC) model to fit the experimental results (except of that with the pristine Al cathode). Electron-only currents in disordered organic semiconductors are commonly modeled using analogues of Child's Law,[70] which describes single carrier currents in a trap-free insulator and predicts that the current density (J) varies by the square of the applied bias (V) and inversely by the cube of the film thickness (L) according to eq 1:

DOI: 10.1021/jacs.5b01889
J. Am. Chem. Soc. 2015, 137, 6844–6856

Table 1. Device Characteristics of OPV 1 Having the Device Configuration ITO/MoO_x/P3HT:$PC_{71}BM$/Cathode with Varying Cathode Configurations[a]

OPV 1 (P3HT:$PC_{71}BM$)						
cathode	J_{sc} (mA/cm^2)	V_{oc} (V)	FF	PCE (%)	R_s (Ω cm^2)	R_{sh} (Ω cm^2)
Al	8.8(±0.20)	0.57(±0.01)	0.57(±0.02)	2.9(±0.15)	4.3	950
MeOH/Al	9.0(±0.15)	0.60(±0.01)	0.58(±0.01)	3.1(±0.15)	3.5	1100
Cs_2CO_3/Al	9.3(±0.15)	0.58(±0.01)	0.59(±0.01)	3.2(±0.10)	3.2	1150
POM 1/Al	9.8(±0.15)	0.63(±0.01)	0.60(±0.01)	3.7(±0.15)	2.1	1800
POM 2/Al	9.9(±0.10)	0.63(±0.01)	0.60(±0.01)	3.8(±0.10)	2.0	1800
POM 3/Al	10.0(±0.15)	0.64(±0.01)	0.61(±0.01)	3.9(±0.10)	1.9	1850
POM 4/Al	10.0(±0.10)	0.64(±0.01)	0.60(±0.01)	3.8(±0.10)	1.9	1900
POM 5/Al	10.4(±0.10)	0.65(±0.01)	0.61(±0.01)	4.1(±0.10)	1.7	1900
POM 6/Al	10.5(±0.10)	0.65(±0.01)	0.61(±0.01)	4.2(±0.15)	1.6	2000

[a]Mean values and standard deviations were extracted from a batch of 24 devices.

$$J = \frac{9}{8}\varepsilon_0\varepsilon_r\mu_e\frac{V^2}{L^3} \quad (1)$$

where ε_r is the dielectric permittivity and μ_e is the electron mobility of the active layer. Note that to include the electric field dependency of the mobility, eq 1 can be appropriately modified according to the Mott−Gurney law (eq2):

$$J = \frac{9}{8}\varepsilon_0\varepsilon_r\mu_{e,0}\frac{V^2}{L^3}\exp\left[0.89\beta\left(\frac{V}{L}\right)^{1/2}\right] \quad (2)$$

where $\mu_e = \mu_{e,0}\exp[\beta(V/L)^{1/2}]$ (Poole−Frenkel mobility law), $\mu_{e,0}$ is the zero-field mobility, and β is the field activation factor of the mobility. From Figure 5c, the calculated electron mobility in devices with the POM layers were 5.1×10^{-3} cm^2 V^{-1} s^{-1}, which is among the highest reported values for F8BT,[71] whereas the electron mobility extracted from the $J-V$ characteristic of the Cs_2CO_3 based F8BT-device was 4.0×10^{-3} cm^2 V^{-1} s^{-1}.

The enhanced electron mobility and remarkable overall device performance following POM deposition on the emissive OSC originates from the formation of a better (Ohmic) contact at the cathode interface and from the reduced electron injection barrier, as illustrated in the energy level diagram of the F8BT-based OLED, shown in Figure 5d. The W_F of ITO was calculated from the secondary electron cutoff UPS spectrum (Figure S6) whereas the energy levels of the different layers of the OLED were estimated from the UPS spectra measured after each deposition; the energy gap values of those materials were previously measured.[65] It is observed that with the absence of POM interlayer a large electron injection barrier of ∼0.8 eV (equal to the energy difference between the LUMO of F8BT (3.5 eV) and the W_F of Al (4.3 eV)) significantly prohibits the injection of electrons, especially at low voltages as it can be clearly seen in Figure 5c. After inserting the POM interlayer on top of F8BT a vacuum level shift occurs, which forces the LUMO of F8BT to match well with the LUMO, more probably, the upper LUMOs of POM. Taking into account the occupancy of these LUMO levels of POMs, due to its spontaneous reduction by Al, we conclude that electrons might freely move from the LUMO level of POM, which is now aligned to the LUMO of F8BT, and inject into the latter even at very low forward voltages. Thus, the interfacial modification of the F8BT/Al junction using a POM interlayer creates an Ohmic contact through changes in the energy barrier for electron injection. This ideal Ohmic contact promotes overall electron transport and provides high electron mobility pathways. Note that, an Ohmic contact is expected to be formed at the anode ITO/MoO_x/F8BT junctions (Figure 5d),[64,65] contributing also to the remarkable performance of our devices.

POMs as Electron Extraction Layers in OPVs. Next, we investigated the effect of incorporating the reduced POMs as electron extraction layers (EELs) in bulk heterojunction (BHJ) OPVs based on different donors, such as the well-known P3HT,[72] and the recently introduced small band gap PCDTBT and PTB7,[73,74] which were selected due to the high efficiencies they can yield resulting from their ability to harvest a wider range of the solar spectrum and to deliver a high open-circuit voltage when blended with our $PC_{71}BM$ acceptor. The device structure was again ITO/MoO_x/active layer/EEL/Al and is shown in Figure 6a, where the chemical structures of organic semiconductors used in our OPVs, are also presented. The current density−voltage ($J-V$) characteristics under simulated 1.5 AM solar irradiation of P3HT:$PC_{71}BM$-based devices (OPV 1) using POMs as EELs are shown in Figure 6b, while Table 1 summarizes the devices operational characteristics (mean values and standard deviations). Except of the POM bearing devices three reference devices were also fabricated, two of them using either a pristine Al or a Cs_2CO_3/Al cathode and the third having exposed the photoactive layer to a methanol (MeOH) solvent prior the deposition of Al. This was deemed necessary as there are reports of improved cell characteristics with MeOH treatment of the photoactive layer,[75] and because POMs and Cs_2CO_3 have been deposited from MeOH solutions. From the $J-V$ curves becomes evident that the reference device exhibits a power conversion efficiency (PCE) of 2.9%, whereas those with the Cs_2CO_3/Al cathode (PCE = 3.2%) and the MeOH treatment (PCE = 3.1%) operate better due to the enhancement of the device short-circuit current (J_{sc}) and open-circuit voltage (V_{oc}), respectively. However, the devices with the POM/Al cathodes exhibit higher PCE values in the range of 3.7−4.2% (the highest PCEs were achieved in the devices with the highly reduced POMs 5 and 6) which cannot be considered as a net MeOH solution effect. It can be seen that the efficiency enhancement is a direct result of highly improved J_{sc}, V_{oc} and also fill factor (FF) in our POM incorporating devices. The large enhancement of J_{sc} and FF is also reflected in the considerable reduction of the series resistance, R_s, of POM bearing devices compared with the reference ones (Table 1) as extracted from dark current measurements (Figure S8). Reduced R_s suggests improved contact between the active layer and the cathodes contact, which facilitates electron transport/extraction and therefore enhanced J_{sc} and FF of the

DOI: 10.1021/jacs.5b01889
J. Am. Chem. Soc. 2015, 137, 6844−6856

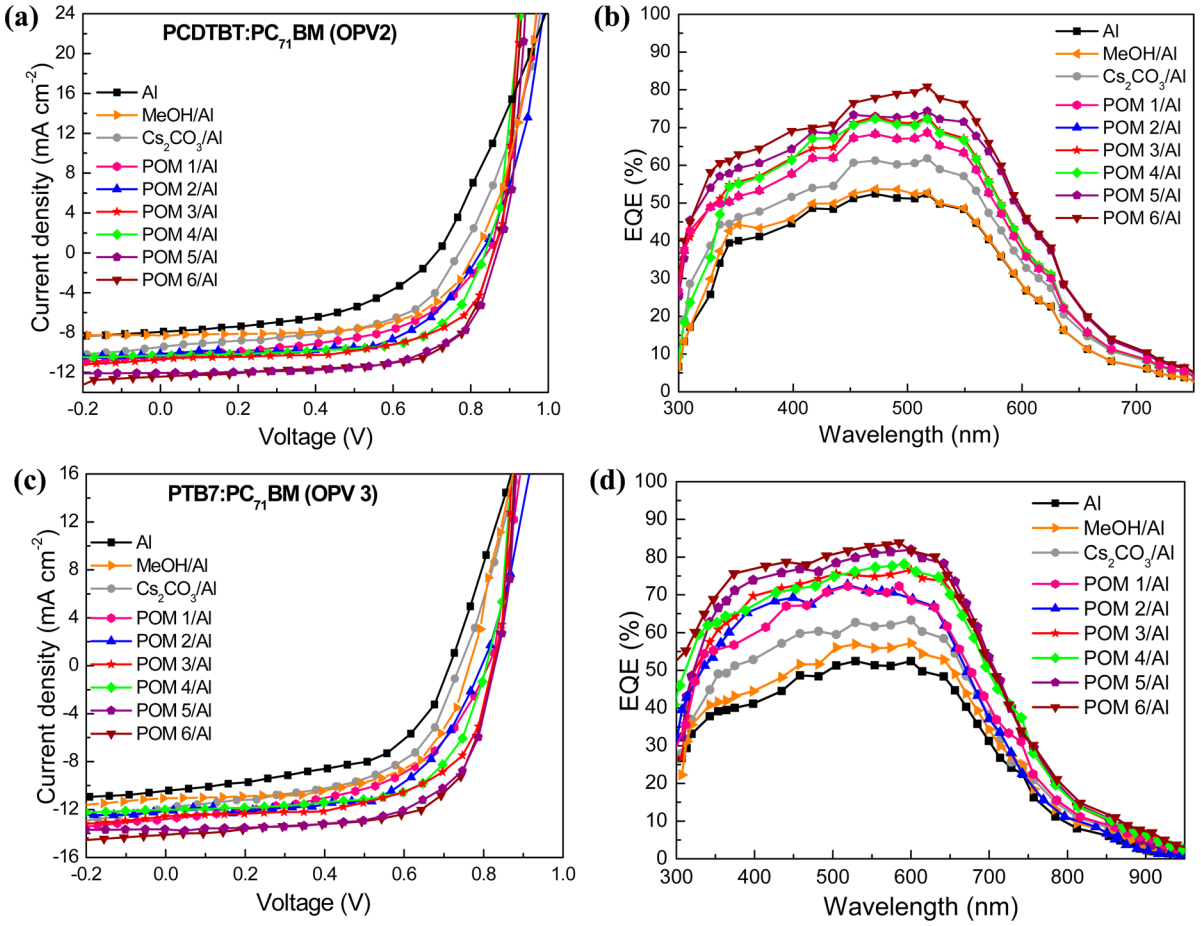

Figure 7. (a) $J-V$ characteristics under AM 1.5 illumination of OPV 2 devices based on PCDTBT:$PC_{71}BM$ blend with various cathode interfaces. (b) The corresponding EQE curves in the wavelength range from 300 to 700 nm. (c) $J-V$ characteristics under AM 1.5 illumination of OPV 3 devices based on PTB7:$PC_{71}BM$ blend with various cathode interfaces. (d) The corresponding EQE curves in the wavelength range from 300 to 900 nm.

devices with POMs as compared with the reference ones.[76] On the contrary, in the reference devices (especially in that with the pristine Al cathode) an increased contact barrier makes the extraction of electrons more difficult toward the cathode and reduces the device performance. The external quantum efficiency (EQE) spectra of the devices with different cathode contacts are shown in Figure 6c. The devices with the POM/Al cathode exhibited higher values, from 350 to 550 nm, than the reference ones. The device with the POM 6 interlayer showed the highest EQE with a maximum value of 84% at 460 nm, which represents a 50% improvement compared to 56% of the reference device with the pristine Al cathode. This enhancement in EQEs suggests that the photon-to-electron conversion processes are very efficient in the POM modified devices owing to the stronger electron extraction/transport capability of the latter. The effect of inserting POMs at the cathode interface on electron transport efficiency was further confirmed by the electron-only device characteristic. Figure 6d shows the measured $J-V$ characteristics in a log−log scale. It is observed that with the POM interlayers the J at 1 V is 3 orders of magnitude larger than that of the reference device without any interlayer whereas the J of the other two reference devices (although higher than that of the device with the pristine Al cathode) is significantly lower than that of the POM modified devices. Those results indicate a low or even negligible electron extraction barrier at the interface between the photoactive layer and the Al contact. The $J-V$ characteristics were fitted with the SCLC model (eq 2) and thus the electron mobility was calculated for each device (Table S2). It is observed that the devices with the POM/Al cathodes showed the highest mobility (3.4×10^{-3} cm^2 V^{-1} s^{-1}), which corresponds to an approximately 3-fold increase compared to the device with the pristine Al cathode (1.2×10^{-3} cm^2 V^{-1} s^{-1}). This result indicates that the deposition of POMs on the photoactive layer effectively promoted electron transport and extraction eliminating the electron extraction barrier and can explain the enhanced J_{sc} and FF obtained in the POM modified devices. In addition, the V_{oc} of all OPV devices using POMs as EELs is significantly enhanced. To better understand the origin of V_{oc} increase in the POM modified devices we obtained the Mott−Schottky characteristics (C^{-2}−V) of our devices (Figure S9 and relevant discussion), which revealed that the built-in voltage (V_{bi}) is significantly reinforced in the devices with POM interlayers. Increase of the V_{bi} will increase the device electric field strength, leading to a decrease in carrier recombination and an increase in V_{oc} (as well as J_{sc} and FF).[76,77]

Next, transient photocurrent (TPC) measurements were performed to study the photocarrier decay dynamics under an extraction field for the devices with POM interlayers and for the reference ones. Through applying an external DC bias we can change the internal field and we can alter the amount of time the carriers spend in the device prior to extraction and is

DOI: 10.1021/jacs.5b01889
J. Am. Chem. Soc. 2015, 137, 6844−6856

Table 2. Characteristics of Devices OPV 2: ITO/MoO_x/PCDTBT:$PC_{71}BM$/Cathode and OPV 3: ITO/MoO_x/PTB7:$PC_{71}BM$/Cathode with Varying Cathode Configurations[a]

OPV 2 (PCDTBT:$PC_{71}BM$)					OPV 3 (PTB7:$PC_{71}BM$)				
cathode	J_{sc} (mA/cm^2)	V_{oc} (V)	FF	PCE (%)	cathode	J_{sc} (mA/cm^2)	V_{oc} (V)	FF	PCE (%)
Al	9.8(±0.20)	0.82(±0.10)	0.57(±0.10)	4.7(±0.25)	Al	12.3(±0.25)	0.68(±0.10)	0.58(±0.10)	4.8(±0.25)
MeOH/Al	9.9(±0.20)	0.86(±0.10)	0.62(±0.10)	5.3(±0.20)	MeOH/Al	12.3(±0.25)	0.72(±0.10)	0.62(±0.10)	5.5(±0.25)
Cs_2CO_3	10.5(±0.15)	0.84(±0.10)	0.61(±0.10)	5.5(±0.15)	Cs_2CO_3	13.0(±0.20)	0.70(±0.10)	0.62(±0.10)	5.6(±0.20)
POM 1	11.5(±0.20)	0.87(±0.10)	0.64(±0.10)	6.1(±0.20)	POM 1	13.6(±0.15)	0.74(±0.10)	0.65(±0.10)	6.5(±0.25)
POM 2	11.5(±0.15)	0.87(±0.10)	0.64(±0.10)	6.1(±0.15)	POM 2	13.6(±0.15)	0.75(±0.10)	0.65(±0.10)	6.6(±0.20)
POM 3	12.0(±0.15)	0.88(±0.10)	0.65(±0.10)	6.9(±0.15)	POM 3	14.0(±0.15)	0.76(±0.10)	0.67(±0.10)	7.1(±0.20)
POM 4	12.0(±0.15)	0.87(±0.10)	0.64(±0.10)	6.7(±0.15)	POM 4	14.0(±0.15)	0.76(±0.10)	0.66(±0.10)	7.0(±0.20)
POM 5	12.5(±0.10)	0.88(±0.10)	0.66(±0.10)	7.3(±0.15)	POM 5	14.5(±0.15)	0.77(±0.10)	0.68(±0.10)	7.6(±0.15)
POM 6	12.7(±0.15)	0.88(±0.10)	0.66(±0.10)	7.4(±0.15)	POM 6	14.7(±0.15)	0.77(±0.10)	0.68(±0.10)	7.7(±0.15)

[a]Mean values and standard deviations were extracted from a batch of 24 devices.

therefore possible to observe carrier recombination dynamics in these systems.[77] Figure 6e shows the TPC traces for the different devices while they are operating at their maximum power point (500 mV applied bias). The device is under constant illumination of the solar simulator while a small perturbation is given by a pulse laser to introduce a small photocurrent. The single exponential decay of the transient photocurrent perturbation for our devices are due to photogenerated carriers recombining either in the bulk or at the Al/photoactive layer interface. Since these devices have the same hole extraction contact and the same photoactive layer, the difference in carrier lifetime must be due to the difference in the cathode contact. The results indicate that the photogenerated carriers recombine at a faster rate in the reference devices, especially in that with the bare Al contact. Upon insertion of the Cs_2CO_3 layer or MeOH treatment, carrier recombination at the cathode/photoactive layer interface was reduced resulting in a longer carrier lifetime and better device performance. However, the reduction in carrier recombination is superior when inserting the POM interlayers at the cathode/photoactive layer interface where a large increase in carrier lifetime was observed. The observed enhancement in carrier lifetime in the POM modified devices indicates that carrier density inside those devices is decreased (since photogenerated electrons are easily swept toward the cathode electrode due to the reduced electron extraction barrier and the increased internal field strength), resulting in a lower rate of bimolecular recombination. Note that the better quality of the cathode contact of our POM modified devices results also in their superior environmental stability as compared to the reference ones (Figure S10).

On the basis of all the above experimental evidence we conclude that significant gains in the cell efficiency when using the reduced POMs can be achieved. A reasonable question however is whether these materials are appropriate for use in devices with various donor:acceptror combinations in the photoactive blend. To demonstrate the universality of using POM EELs in OPV cells, we also fabricated devices with the photoactive blend being either the PCDTBT:$PC_{71}BM$ (OPV 2) or the PTB7:$PC_{71}BM$ (OPV 3). The $J-V$ characteristics (under simulated 1.5 AM solar irradiation) of OPV 2 and OPV 3 devices are shown in Figures 7a and c, respectively, whereas the EQEs of the same devices are also shown in Figures 7b and d, respectively. Table 2 summarizes the devices operational characteristics. The reference OPV 2 shows a PCE of 4.7% while the reference OPV 3 exhibits a PCE of 4.8%. Again, the POM modified devices showed a progressive enhancement in their operational characteristics reaching high values, with the highest efficiencies to be obtained in the devices with the highly reduced POMs 5 and 6 interlayers. In particular, our champion PCDTBT:$PC_{71}BM$-based device using POM 6 as the EEL exhibits the high PCE values of 7.4% whereas in the case of PTB7:$PC_{71}BM$ based device with the POM 6/Al cathode a PCE of 7.7% is achieved. Similarly, the EQE values of the POM modified devices were always higher than those of the reference ones in the whole spectral region. All these results strengthen our conclusion about reduced POMs being effective and also universal cathode interlayers which greatly improve electron injection/extraction efficiency and reduce recombination losses when embedded in OLED/OPV devices. We keep in mind that POMs are easily produced chemical species and, therefore, could become routine tools of high-throughput and widespread application of not only organic optoelectronics but also in other devices requiring highly effective cathode interfaces.

CONCLUSIONS

In summary, we show here that Keggin and Dawson polyoxometalate (POM) films can be readily reduced at their interface with an Al electrode and that the degree of reduction is strongly affected by the position of their LUMO level. It was found that substitution of the metal centers in a Keggin structure with other more electronegative ones or/and transition to a Dawson structure results in a higher degree of reduction due to the decrease of the LUMO energy. We also demonstrate the application of reduced POMs as cathode interlayers in organic optoelectronic devices, such as OLEDs and OPVs using a wide range of organic semiconductors as the active components. Significant device performance enhancement was achieved when incorporating the reduced POMs at organic active layer/Al cathode interfaces, which was dependent on the degree of their reduction. This enhancement was attributed to enhanced electron injection/extraction efficiency and reduced recombination losses owing to a large decrease of the electron injection/extraction barrier and improved electron transport. These results suggest that the solid state electrochemistry of POMs enables the formation of promising cathode materials in high performance organic optoelectronics, but also in diverse applications such as photocatalytic devices and fuel cells.

DOI: 10.1021/jacs.5b01889
J. Am. Chem. Soc. 2015, 137, 6844−6856

■ ASSOCIATED CONTENT

Supporting Information

Additional figures (Figures S1−S10) and relevant discussion as noted in text. The Supporting Information is available free of charge on the ACS Publications website at DOI: 10.1021/jacs.5b01889.

■ AUTHOR INFORMATION

Corresponding Author

*mariva@imel.demokritos.gr

Notes

The authors declare no competing financial interest.

■ ACKNOWLEDGMENTS

The project "Implementing advanced interfacial engineering strategies for highly efficient hybrid solar cells" (Acronym: IMAGINE-HYSOL) is implemented under the "ARISTEIA II" Action of the "Operational Programme Education and Lifelong Learning" and is cofunded by the European Social Fund (ESF) and National Resources.

■ REFERENCES

(1) Yu, G.; Gao, J.; Hummelen, J. C.; Wudl, F.; Heeger, A. J. *Science* **1995**, *270*, 1789.
(2) Blom, P. W. M.; Mihailetchi, V. D.; Koster, L. J. A.; Markov, D. E. *Adv. Mater.* **2007**, *19*, 1551.
(3) Dennler, G.; Scharber, M. C.; Brabec, C. J. *Adv. Mater.* **2009**, *21*, 1323.
(4) Ma, H.; Yip, H.-L.; Huang, F.; Jen, A. K.-Y. *Adv. Funct. Mater.* **2010**, *20*, 1371.
(5) Tang, J. S C. W.; Vanslyke, S. A. *Appl. Phys. Lett.* **1987**, *51*, 913.
(6) Greenham, N. C.; Moratti, S. C.; Bradley, D. D. C.; Friend, R. H.; Holmes, A. B. *Nature* **1993**, *365*, 628.
(7) Reineke, S.; Lindner, F.; Schwartz, G.; Seidler, N.; Walzer, K.; Lussem, B.; Leo, K. *Nature* **2009**, *459*, 234.
(8) Friend, R. H.; Gymer, R. W.; Holmes, A. B.; Burroughes, J. H.; Marks, R. N.; Taliani, C.; Bradley, D. D. C.; Dos Santos, D. A.; Bredas, J. L.; Logdlund, M.; Salaneck, W. R. *Nature* **1999**, *397*, 121.
(9) Zaumseil, J.; Friend, R. H.; Sirringhaus, H. *Nat. Mater.* **2006**, *5*, 69.
(10) Gong, X.; Robinson, M. R.; Ostrowski, J. C.; Moses, D.; Bazan, G. C.; Heeger, A. J. *Adv. Mater.* **2002**, *14*, 581.
(11) So, F.; Krummacher, B.; Mathai, M. K.; Poplavskyy, D.; Choulis, S. A.; Choong, V. E. *J. Appl. Phys.* **2007**, *102*, 091101.
(12) Ha, Y. E.; Jo, M. Y.; Park, J.; Kang, Y.-C.; Yoo, S. I.; Kim, J.-H. *J. Phys. Chem. C* **2013**, *117*, 2646.
(13) Melnick, D. A. *J. Chem. Phys.* **1957**, *26*, 1136.
(14) Zhou, Y.; Cheun, H.; Potscavage, W. J., Jr; Fuentes-Hernandez, C.; Kim, S.-J.; Kippelen, B. *J. Mater. Chem.* **2010**, *20*, 6189.
(15) Bok Kim, J.; Ahn, S.; Ju Kang, S.; Nuckolls, C.; Loo, Y.-L. *Appl. Phys. Lett.* **2013**, *102*, 103302.
(16) Zhou, Y.; Fuentes-Hernandez, C.; Shim, J.; Meyer, J.; Giordano, A. J.; Li, H.; Winget, P.; Papadopoulos, T.; Cheun, H.; Kim, J.; Fenoll, M.; Dindar, A.; Haske, W.; Najafabadi, E.; Khan, T. M.; Sojoudi, H.; Barlow, S.; Graham, S.; Bredas, J.-L.; Marder, S. R.; Kahn, A.; Kippelen, B. *Science* **2012**, *336*, 327.
(17) Bulliard, X.; Ihn, S.-G.; Yun, S.; Kim, Y.; Choi, D.; Choi, J.-Y.; Kim, M.; Sim, M.; Park, J.-H.; Choi, W.; Cho, K. *Adv. Funct. Mater.* **2010**, *20*, 4381.
(18) Khodabakhsh, S.; Sanderson, B. M.; Nelson, J.; Jones, T. S. *Adv. Funct. Mater.* **2006**, *16*, 95.
(19) Vasilopoulou, M.; Georgiadou, D. G.; Douvas, A. M.; Soultati, A.; Constantoudis, V.; Davazoglou, D.; Gardelis, S.; Palilis, L. C.; Fakis, M.; Kennou, S.; Lazarides, T.; Coutsolelos, A. G.; Argitis, P. *J. Mater. Chem. A* **2014**, *2*, 182.
(20) Yoon, S. M.; Lou, S. J.; Loser; Smith, J.; Chen, L. X.; Facchetti, A.; Marks, T. *Nano Lett.* **2012**, *12*, 6315.
(21) Huang, J.; Xu, Z.; Yang, Y. *Adv. Funct. Mater.* **2007**, *17*, 1966.
(22) Zilberberg, K.; Behrendt, A.; Kraft, M.; Scherf, U.; Riedl, T. *Org. Electron.* **2013**, *14*, 951.
(23) Kang, H.; Hong, S.; Lee, J.; Lee, K. *Adv. Mater.* **2012**, *24*, 3005.
(24) Liu, X. F.; Wen, W.; Bazan, G. C. *Adv. Mater.* **2012**, *24*, 4505.
(25) Zhou, H.; Zhang, Y.; Seifter, J.; Collins, S. D.; Luo, C.; Bazan, C. G.; Nguyen, T.-Q.; Heeger, A. J. *Adv. Mater.* **2013**, *25*, 1646.
(26) Lee, B. R.; Jung, E. D.; Park, J. S.; Nam, Y. S.; Min, S. H.; Kim, B.-S.; Lee, K.-M.; Jeong, J.-R.; Friend, R. H.; Kim, J.-S.; Kim, S. O.; Song, M. H. *Nat. Commun.* **2014**, *5*, 4840.
(27) Hill, C. L. *Chem. Rev.* **1998**, *98*, 1.
(28) Gouzerh, P.; Che, M. *Actual. Chim.* **2006**, *298*, 9.
(29) Keggin, J. F. *Nature* **1933**, *131*, 908.
(30) Dawson, B. *Acta Crystallogr.* **1953**, *6*, 113.
(31) Rhule, J. T.; Neiwert, W. A.; Hardcastle, K. I.; Do, B. T.; Hill, G. L. *J. Am. Chem. Soc.* **2001**, *123*, 12101.
(32) Keita, B.; Kortz, U.; Holzle, L. R. B.; Brown, S.; Nadjo, L. *Langmuir* **2007**, *23* (19), 9531.
(33) Long, D.-L.; Streb, C.; Song, Y.-F.; Mitchell, S.; Cronin, L. *J. Am. Chem. Soc.* **2008**, *130*, 1830.
(34) Long, D.-L.; Kogerler, P.; Cronin, L. *Angew. Chem., Int. Ed.* **2004**, *43*, 1817.
(35) Nohra, B.; El Moll, H.; Albelo, L. M. R.; Mialane, P.; Marrot, J.; Mellot-Draznieks, C.; O'Keeffe, M.; Ngo Biboum, R.; Lemaire, J.; Keita, B.; Nadjo, L.; Dolbecq, A. *J. Am. Chem. Soc.* **2011**, *133* (34), 13363.
(36) Neumann, R.; Dahan, M. *Nature* **1997**, *388*, 353.
(37) Macht, J.; Janik, M. J.; Neurock, M.; Inglesia, E. *Angew. Chem.* **2007**, *119*, 8010.
(38) Compain, J.-D.; Mialane, P.; Dolbecq, A.; Mbomekalle, I. M.; Marrot, J.; Secheresse, F.; Riviere, E.; Rogez, G.; Wernsdorfer, W. *Angew. Chem.* **2009**, *121*, 3123.
(39) Wang, H.; Hamanaka, S.; Nishimoto, Y.; Irle, S.; Yokoyama, T.; Yoshikawa, H.; Awaga, K. *J. Am. Chem. Soc.* **2012**, *134*, 4918.
(40) Nishimoto, Y.; Yokoyama, T.; Yoshikawa, H.; Awaga; Irle, S. *J. Am. Chem. Soc.* **2014**, *136*, 9042.
(41) Palilis, L. C.; Vasilopoulou, M.; Georgiadou, D. G.; Argitis, P. *Org. Electron.* **2010**, *11*, 887.
(42) Palilis, L. C.; Vasilopoulou, M.; Douvas, A. M.; Georgiadou, D. G.; Kennou, S.; Stathopoulos, N. A.; Constantoudis, V.; Argitis, P. *Sol. Energy Mater. Sol. Cells* **2013**, *114*, 205.
(43) Yang, Y.; Xu, L.; Li, F.; Du, K.; Sun, Z. *J. Mater. Chem.* **2010**, *20*, 10835.
(44) Alaaeddine, M.; Zhu, Q.; Fichou, D.; Izzet, G.; Rault, J. E.; Barrett, N.; Proust, A.; Tortech, L. *Inorg. Chem. Front.* **2014**, *1*, 682.
(45) Zhu, Y.; Yuan, Z.; Cui, W.; Wu, Z.; Sun, Q.; Wang, S.; Kang, Z.; Sun, B. *J. Mater. Chem. A* **2014**, *2*, 1436.
(46) Jia, X.; Shen, L.; Yao, M.; Liu, Y.; Yu, W.; Guo, W.; Ruan, S. *ACS Appl. Mater. Interfaces* **2015**, *7*, 5367.
(47) Douvas, A. M.; Makarona, E.; Glezos, N.; Argitis, P.; Mielczarski, J. A.; Mielczarski, E. *ACS Nano* **2008**, *2*, 733.
(48) Soultati, A.; Douvas, A. M.; Georgiadou, D. G.; Palilis, L. C.; Bein, T.; Feckl, J. M.; Gardelis, S.; Fakis, M.; Kennou, S.; Falaras, P.; Stergiopoulos, T.; Stathopoulos, N. A.; Davazoglou, D.; Argitis, P.; Vasilopoulou, M. *Adv. Energy Mater.* **2014**, *4*, 1300896.
(49) Pope, M. T.; Yamase, T. *Polyoxometalate Chemistry for Nanocomposite Design*; Kluwer: Dordrecht, 2002.
(50) Compain, J.-D.; Mialane, P.; Dolbecq, A.; Mbomekalle, I. M.; Marrot, J.; Sécheresse, F.; Riviere, E.; Rogez, G.; Wernsdorfer, W. *Angew. Chem., Int. Ed.* **2009**, *48*, 3077.
(51) Mizuno, N.; Yamaguchi, K.; Kamata, K. *Coord. Chem. Rev.* **2005**, *249*, 1944.
(52) Rhule, J. T.; Hill, C. L.; Judd, D. A. *Chem. Rev.* **1998**, *98*, 327.
(53) Pope, M. T.; Muller, A. *Angew. Chem., Int. Ed. Engl.* **1991**, *30*, 34.
(54) Papaconstantinou, E.; Pope, M. T. *Inorg. Chem.* **1970**, *9*, 667.
(55) Duclusaud, H.; Borshch, S. A. *J. Am. Chem. Soc.* **2001**, *123*, 2825.

DOI: 10.1021/jacs.5b01889
J. Am. Chem. Soc. 2015, 137, 6844−6856

(56) López, X.; Bo, C.; Poblet, J. M. *J. Am. Chem. Soc.* **2002**, *124*, 12574.
(57) Andres, H.; Clemente-Juan, J. M.; Basler, R.; Aebersold, M.; Gudel, H.-U.; Borras- Almenar, J. J.; Gaita, A.; Coronado, E.; Buttner, H.; Janssen, S. *Inorg. Chem.* **2001**, *40*, 1943−1950.
(58) Maestre, J. M.; Lopez, X.; Bo, C.; Casan-Pastor, N.; Poblet, J. M. *J. Am. Chem. Soc.* **2001**, *123*, 3749.
(59) Lopez, X.; Maestre, J. M.; Bo, C.; Poblet, J. M. *J. Am. Chem. Soc.* **2001**, *123*, 9571.
(60) Proust, A.; Robert, F.; Gouzerh, P.; Chen, Q.; Zubieta, J. *J. Am. Chem. Soc.* **1997**, *119*, 3523.
(61) Varga, G. M.; Papaconstantinou, E.; Pope, M. T. *Inorg. Chem.* **1970**, *9*, 662.
(62) Barreca, D.; Carta, G.; Gasparotto, A.; Rossetto, G.; Tondello, E.; Zanella, P. *Surf. Sci. Spectra* **2001**, *8*, 258.
(63) Chen, Y.; Xie, K.; Liu, Z. *Appl. Surf. Sci.* **1998**, *126*, 347.
(64) Greiner, M. T.; Helander, M. G.; Tang, W.-M.; Wang, Z.-B.; Qiu, J.; Lu, Z.-H *Nat. Mater.* **2012**, *11*, 76.
(65) Vasilopoulou, M.; Douvas, A. M.; Georgiadou, D. G.; Palilis, L. C.; Kennou, S.; Sygellou, L.; Soultati, A.; Kostis, I.; Papadimitropoulos, G.; Davazoglou, D.; Argitis, P. *J. Am. Chem. Soc.* **2012**, *134*, 16178.
(66) Miras, H. N.; Yan, J.; Long, D.-J.; Cronin, L. *Chem. Soc. Rev.* **2012**, *41*, 7403.
(67) Muller, A.; Peters, F.; Pope, M. T.; Gatteschi, D. *Chem. Rev.* **1998**, *98*, 239.
(68) Png, R.-Q.; Chia, P.-J.; Tang, J.-C.; Liu, B.; Sivaramakrishnan, S.; Zhou, M.; Khong, S.-H.; Chan, H. S. O.; Burroughess, J. H.; Chua, L.-L.; Friend, R. H.; Ho, P. K. H. *Nat. Mater.* **2010**, *9*, 152.
(69) Fang, J.; Wallikewitz, B. H.; Gao, F.; Tu, G.; Müller, C.; Pace, G.; Friend, R. H.; Huck, W. T. S. *J. Am. Chem. Soc.* **2011**, *133*, 683 68.
(70) He, Z.; Zhong, C.; Huang, X.; Wong, W.-Y.; Wu, H.; Chen, L.; Su, S.; Cao, Y. *Adv. Mater.* **2011**, *23*, 4636.
(71) Donley, C. L.; Zaumseil, J.; Andreasen, J. W.; Nielsen, M. M.; Sirringhaus, H.; Friend, R. H.; Kim, J. S. *J. Am. Chem. Soc.* **2005**, *127*, 12890.
(72) Staniec, P. A.; Parnell, A. J.; Dunbar, A. D. F.; Yi, H.; Pearson, A. J.; Wang, T.; Hopkinson, P. E.; Kinane, C.; Dalgliesh, R. M.; Donald, A. M.; Ryan, A. J.; Iraqi, A.; Jones, R. A. L.; Lidzey, D. G. *Adv. Energy Mater.* **2011**, *1*, 499.
(73) He, Z.; Xiao, B.; Liu, F.; Wu, H.; Yang, Y.; Xiao, S.; Wang, C.; Russell, T. P.; Cao, Y. *Nat. Photonics* **2015**, *9*, 174.
(74) Zhang, Z.-G.; Qi, B.; Jin, Z.; Chi, D.; Qi, Z.; Li, Y.; Wang, J. *Energy Environ. Sci.* **2014**, *7*, 1966.
(75) Zhou, H.; Zhang, Y.; Seifter, J.; Collins, S. D.; Luo, C.; Bazan, G. C.; Ngyen, T.-Q.; Heeger, A. J. *Adv. Mater.* **2013**, *25*, 1646.
(76) Lai, T.-H.; Tsang, S.-W.; Manders, J. R.; Chen, S.; So, F. *Mater. Today* **2013**, *16*, 424.
(77) Tiwana, P.; Docampo, P.; Johnston, M. B.; Herz, L. M.; Snaith, H. J. *Energy Environ. Sci.* **2012**, *5*, 9566.

DOI: 10.1021/jacs.5b01889
J. Am. Chem. Soc. 2015, 137, 6844−6856